A Letters Journal Exploring
the Frontiers of Physics

OFFPRINT

Nonlinear plasma waves and wavebreaking in quantum plasmas

A. Schmidt-Bleker, W. Gassen and H.-J. Kull

EPL, **95** (2011) 55003

A Letters Journal Exploring the Frontiers of Physics

September 2011

EPL, **95** (2011) 55003
doi: 10.1209/0295-5075/95/55003

www.epljournal.org

Nonlinear plasma waves and wavebreaking in quantum plasmas

A. Schmidt-Bleker, W. Gassen and H.-J. Kull[(a)]

Institute for Theory of Statistical Physics, RWTH Aachen University - Templergraben 55, 52056 Aachen, Germany, EU

received 28 June 2011; accepted in final form 26 July 2011
published online 9 August 2011

PACS 52.35.-g – Waves, oscillations, and instabilities in plasmas and intense beams
PACS 52.65.-y – Plasma simulation
PACS 36.40.Gk – Plasma and collective effects in clusters

Abstract – The nonlinear evolution of plasma waves in quantum plasmas is studied up to and beyond the wavebreaking limit. Wavebreaking sets basic limitations to hydrodynamic models. In this work, a complete quantum kinetic computational approach is presented. Linear dispersion relations and Landau damping rates can be accurately reproduced by this method. In the nonlinear regime wavebreaking amplitudes in quantum plasmas are obtained and compared to theoretical results. Specific quantum effects can be explained by a nonlinear coupling of plasmon to free-particle modes in the wavebreaking regime.

Quantum plasmas are a generic state of matter at high densities and low temperatures. If the Fermi energy of the electrons exceeds both the average interaction energy and the temperature, a weakly coupled degenerate electron gas is obtained [1]. Dense plasmas occur under various conditions in semi-conductors, metals, metallic clusters, quantum nanostructures, laser-produced solid-state plasmas and in astrophysical objects like white dwarfs. In the past years, spectroscopic measurements on isochorically heated solid-density plasmas became available and plasmons have been experimentally observed in warm dense matter [2]. The present development of coherent brilliant X-ray radiation sources will offer new possibilities for producing and probing extreme states of high-density plasmas [3].

In this work, we focus on the quantum nonlinear evolution of plasma waves. It is well known that the nonlinear propagation of plasma waves has a fundamental limitation given by the wavebreaking threshold. Wavebreaking is important for wave energy dissipation and associated electron heating in collisionless plasmas. Beyond the wavebreaking threshold simple fluid models fail and a more general kinetic treatment by the Vlasov-Maxwell theory is required. Wavebreaking has been found of considerable interest in cold [4], thermal [5–7] and relativistic [8,9] classical plasmas, but apparently the quantum-mechanical wavebreaking limit in dense warm matter has not been considered so far. It is our basic goal to investigate the wavebreaking regime in the framework of quantum kinetic theory. It is of basic theoretical interest due to the underlying violation of both fluid and classical approximations.

In the present paper, we propose a general computational approach, the carrier-envelope wave (CEW) method, for ideal quantum plasmas. Its efficiency proves to be comparable to that of classical particle-in-cell (PIC) plasma simulations [10] and its validity can be well confirmed by theoretical results for linear plasma waves. The CEW method gives a full quantum kinetic treatment of the nonlinear evolution of plasma waves up to and beyond the wavebreaking limit. One of the major achievements of this work is an efficient computational approach to quantum plasmas that opens the way to a better understanding of quantum kinetic phenomena in nonequilibrium plasmas.

Ideal plasmas are fundamentally described by the set of Vlasov-Maxwell equations. Quantum kinetic equations for nonideal plasmas are the Boltzmann equation for quantum gases [11] and more specific quantum kinetic equations, *e.g.*, for plasmas in strong electromagnetic fields [12]. In the framework of linear response theory a well-known theoretical result is the Lindhard dispersion function for ideal quantum plasmas [13–15]. Beyond the linear regime, numerical methods are of major importance. Most previous computational approaches have been based on the Wigner representation of the quantum Vlasov equation [16] and basic concepts of PIC simulations have been adopted in a semi-classical framework [17]. These approaches approximate quantum diffraction effects either by suitably chosen pseudo-potentials [18–20] or

[(a)] E-mail: kull@ilt-extern.fraunhofer.de

by pseudo-particles [21]. Direct numerical solutions of the complete Wigner-Poisson system have been obtained with Fourier-transform and split-operator techniques [22]. However, since the Wigner function is basically defined on a 6d phase space, direct numerical solutions become exceedingly expensive and apparently only 1d calculations have been performed so far [23,24]. Other approximate approaches are based on hydrodynamic [25,26] and multi-stream kinetic models [27,28]. Occasionally, it is also instructive to consider the simpler Schrödinger-Poisson system for a single wave function and its Madelung transform [24,29].

Consider an ideal quantum plasma with electrostatic interaction, described by the quantum Vlasov equation for the single-particle statistical operator ρ and the Poisson equation for the self-consistent electrostatic potential ϕ,

$$i\hbar\partial_t\rho = [H,\rho], \qquad \Delta\phi = -4\pi q(n_e - n_0). \tag{1}$$

Here $H = \frac{\boldsymbol{P}^2}{2m} + q\phi$ is the Hamiltonian for an electron with mass m and charge q in the potential ϕ, $n_e = n_0\,\mathrm{Tr}\{\rho\delta(\boldsymbol{R} - \boldsymbol{r})\}$ is the electron density, n_0 is a reference density in a neutral homogeneous plasma equilibrium, $\boldsymbol{R}$ and $\boldsymbol{P}$ denote position and momentum operators, respectively, and Tr is the trace. It is convenient to scale n_e by n_0, which corresponds to a normalization $\mathrm{Tr}\,\rho = V$ of the trace of ρ to the volume V.

The computational advantage of PIC simulations results from the propagation of a representative set of phase-space points. In analogy to the sampling of the distribution function by representative phase-space points, the statistical operator of a quantum system can be expressed by an ensemble of representative quantum states $|\Psi_s\rangle$, occurring with probabilities w_s, respectively,

$$\rho = \sum_s w_s|\Psi_s\rangle\langle\Psi_s|, \qquad \sum_s w_s = 1. \tag{2}$$

The quantum Vlasov equation in eq. (1) is equivalent to the propagation of the quantum states according to the time-dependent Schrödinger equation (TDSE),

$$i\hbar\partial_t|\Psi_s\rangle = H|\Psi_s\rangle. \tag{3}$$

Calculating the evolution of the quantum states from initial conditions completely determines the evolution of the statistical operator ρ and of the related expectation values $\langle A\rangle = \mathrm{Tr}(\rho A)$ of any single-particle observable A. It is noted that these equations are just the Hartree self-consistent field equations.

In a thermodynamic equilibrium with temperature T and chemical potential μ, the ensemble of single-particle states is given by momentum eigenstates $|\Psi_s\rangle = |\boldsymbol{p}_s\rangle$. In a system with $N = n_0V$ particles the occupation probability of a given state s is given by the Fermi distribution,

$$Nw_s = \frac{1}{e^{\beta(\epsilon_s-\mu)}+1}, \qquad \epsilon_s = \frac{p_s^2}{2m}, \qquad \beta = \frac{1}{T}. \tag{4}$$

In nonequilibrium the plane waves can be generalized to carrier-envelope (CE) waves,

$$\Psi_s(\boldsymbol{r},t) = \psi_s(\boldsymbol{r},t)e^{\frac{i}{\hbar}(\boldsymbol{p}_s\cdot\boldsymbol{r}-\epsilon_s t)}. \tag{5}$$

The carrier waves are sufficient to describe the equilibrium properties in accordance with the Pauli principle. The envelopes $\psi_s(\boldsymbol{r},t)$ have to be self-consistently calculated together with the interaction potential.

An important step of CEW computations consists in a transformation of the Schrödinger equation (3) to the rest frame of the carrier wave. This allows one to calculate all envelopes with about the same numerical resolution. The potential is calculated from the wave functions at their positions in the laboratory frame. Defining the plasma frequency $\omega_p = \sqrt{4\pi q^2 n_0/m}$ and using the units ω_p^{-1} for time and $\sqrt{\hbar/(m\omega_p)}$ for length, the final equations are

$$i\partial_t\psi_s(\boldsymbol{r}',t) = \left[-\frac{1}{2}\Delta' - \phi(\boldsymbol{r}'+\boldsymbol{p}_s t,t)\right]\psi_s(\boldsymbol{r}',t), \tag{6a}$$

$$\Delta\phi(\boldsymbol{r},t) = -1 + \sum_s w_s|\psi_s(\boldsymbol{r}-\boldsymbol{p}_s t,t)|^2, \tag{6b}$$

where $\boldsymbol{r}' = \boldsymbol{r} - \boldsymbol{p}_s t$ denotes positions in the wave frames. Note that the carrier momenta enter these equations just as velocities of potentials and densities. The initial conditions for the envelopes have been taken in the form

$$\psi = A(x)e^{iS(x)}, \qquad n = A^2, \qquad v = \partial_x S. \tag{7}$$

The amplitude A is determined by the density n and the phase S by the velocity v of the stream. This identification can be based on the Madelung fluid representation of the Schrödinger equation. It also follows from the zeroth- and first-order moments of the Wigner distribution derived from eq. (7). Specifically, we assume in the following the initial conditions $A = 1,\ S = (v_0/k)\sin(kx)$ for a velocity perturbation $v_0\cos(kx)$ in a spatially homogeneous plasma.

Quantum plasma computations with CE waves have a number of attractive features. i) The envelopes often vary only weakly with the carrier momenta. It is therefore sufficient to use a coarse-grained description with a limited number of envelopes. This number can be chosen at a given Fermi energy independent of the system size. In the present calculations we have observed rapid convergence of the results for about 50–100 CE waves. ii) The CE waves are calculated in a completely deterministic manner without introducing statistical noise. iii) The waves with different carrier momenta are members of the ensemble. Therefore, they add incoherently to the density. In contrast, any superposition of waves that is present in the envelopes adds coherently, indicating the quantum features of the interaction. iv) Classical particles with

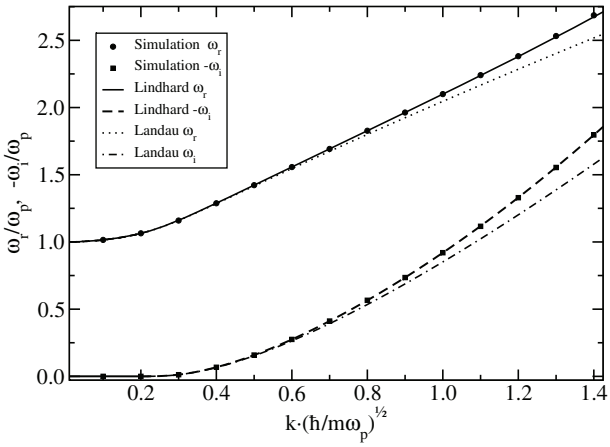

Fig. 1: Frequency ω_r and damping rate $-\omega_i$ of small-amplitude plasma oscillations. The numerical results are compared with corresponding results from the quantum (Lindhard) and classical (Landau) dielectric functions. Parameters: $E_F/\hbar\omega_p = 1.1$, $T/\hbar\omega_p = 1.0$; number of CE waves: 101.

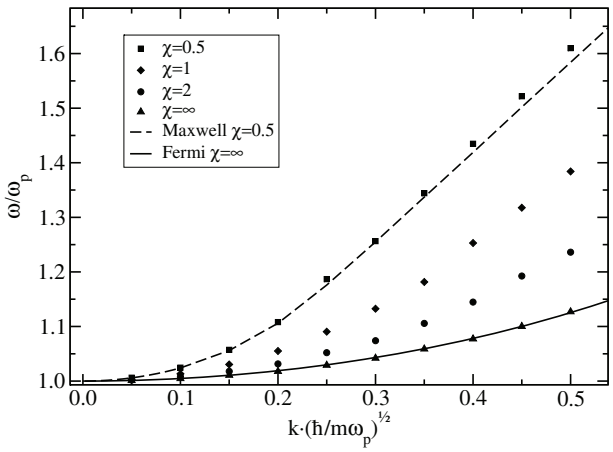

Fig. 2: Frequency ω_r as a function of the degeneracy parameter $\chi = E_F/T$ and corresponding results of the Lindhard dielectric theory for a Fermi and Maxwellian distribution. Parameters: $E_F = 0.8\hbar\omega_p$; number of CE waves: 101.

momentum $\boldsymbol{p}_s$ within some averaging volume $\Delta^3 p_s$ may be viewed as a realization of the density of one CE wave,

$$n_0 w_s |\psi_s(\boldsymbol{r})|^2 \longleftrightarrow f_s(\boldsymbol{r}, \boldsymbol{p}_s)\Delta^3 p_s, \tag{8}$$

where $f_s(\boldsymbol{r}, \boldsymbol{p}_s)$ denotes the classical single-particle distribution function. For each carrier momentum the computational effort of calculating the CE wave by the TDSE is comparable to the classical trajectory calculations for the corresponding particles. In both cases the interaction potential has to be calculated on a spatial grid with about the same numerical resolution.

The numerical method has been validated by calculating the propagation and damping of small amplitude plasma waves. We have solved the set of Schrödinger-Vlasov equations numerically with the Crank-Nicolson scheme [30]. Initial conditions with a sufficiently small velocity amplitude v_0 and periodic boundary conditions have been prescribed. The time evolution of the potential has been fitted to a damped oscillation $\propto e^{\omega_i t}\cos(\omega_r t)$ and thereby the frequency ω_r and damping rates $-\omega_i$ have been determined. As a benchmark problem, a Fermi energy $E_F = 1.1\hbar\omega_p$ and a Maxwellian velocity distribution with temperature $T = \hbar\omega_p$ have been assumed. In fig. 1, the numerical solution is compared with corresponding results obtained from the quantum-mechanical and classical dielectric functions. It can be seen that the CEW method fully accounts for the quantum-mechanical solution including Landau damping. In contrast, PIC simulations would only reproduce the classical results, showing different asymptotes at large wave numbers. In fig. 2, some dispersion relations for finite temperatures are represented as a function of the degeneracy parameter $\chi = E_F/T$. With increasing temperatures the numerical results converge to the theoretical dispersion relation for a Maxwellian distribution. In all cases considered, there is excellent quantitative agreement between the computational and theoretical results, demonstrating the feasibiliy and accuracy of CEW computations.

In the nonlinear evolution, plasma waves are subject to wavebreaking. The wavebreaking criterion was first derived by Dawson for a cold plasma [4]. It occurs when the Lagrangian coordinates $x(a)$ of neighboring fluid elements with initial positions a approach each other, *i.e.* $\mathrm{d}x = (\partial x(a)/\partial a)\,\mathrm{d}a = 0$. For a sinusoidal perturbation the wavebreaking threshold is reached when the amplitude of the velocity perturbation becomes equal to the phase velocity, $v_0 = \omega_p/k$, or, alternatively, when the electric field amplitude becomes equal to $E_{max} = (m/q)\omega_p v_{ph}$. For convenience, these thresholds are written in physical units. In a classical thermal plasma the wavebreaking amplitudes are reduced by the thermal motion of the particles. The wavebreaking amplitudes decrease from E_{max} to zero as the thermal velocity increases from zero up to the phase velocity v_{ph}. The thermal-plasma wavebreaking threshold was first derived by Coffey [5] in the framework of a waterbag model with a uniform velocity distribution within $-v_{max} < v < v_{max}$. The Coffey result is given by

$$(E/E_{max})^2 = 1 + 2\tilde{v} - \frac{\tilde{v}^2}{3} - \frac{8}{3}\sqrt{\tilde{v}}, \tag{9}$$

where $\tilde{v} = v_{max}/v_{ph} = kv_{max}/\omega$ [5]. As seen in fig. 4 (solid line), the wavebreaking amplitudes are monotonically decreasing with v_{max}/v_{ph}.

We have performed CEW calculations of the wavebreaking amplitudes for a one-dimensional Fermi distribution at temperature zero with Fermi velocity v_F. It can be compared to a waterbag model with maximum velocity $v_{max} = v_F$. The wavebreaking threshold was determined by increasing the perturbation amplitude v_0 until wavebreaking was observed within one plasma period after the first occurrence of the density maximum. The criterion for wavebreaking can be defined quite precisely by looking at

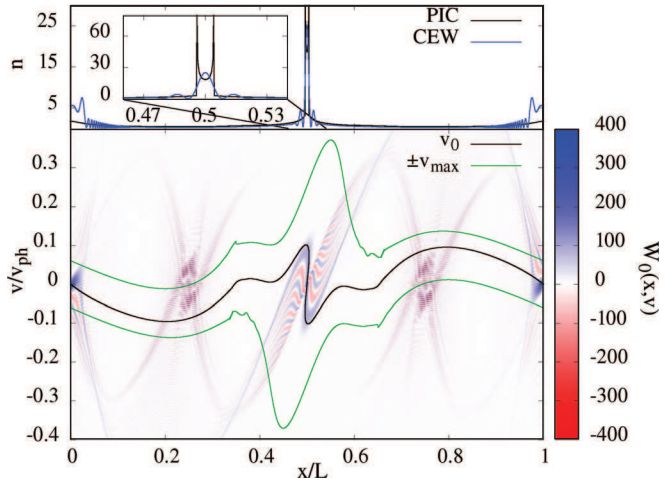

Fig. 3: (Color online) Phase-space (bottom) and density (top) distributions of the zero-momentum CE wave after wavebreaking. Wavebreaking is accompanied by a Z-shaped distortion of the phase-space distribution and by corresponding side maxima in the density. The quantum-mechanical Wigner function (eq. (10) in a.u.) is compared to corresponding classical particle streams (solid lines) with zero and maximum flow velocities. Inset: classical and quantum-mechanical densities in the broken-wave regime. Parameters: $v_{max}/v_{ph} = 0.1$, $E_F/\hbar\omega_p = 2$, $E/E_{max} = 0.75$; number of CE waves or classical particle streams: 51.

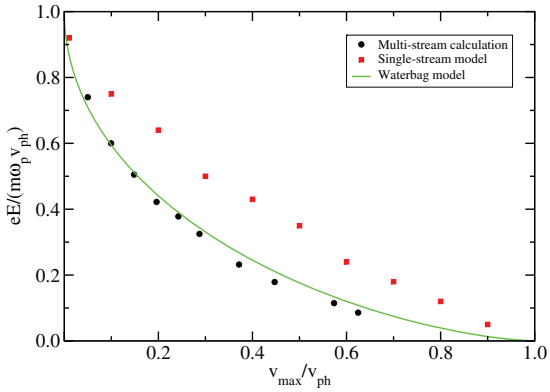

Fig. 4: (Color online) Wavebreaking amplitudes, calculated by the multi-stream CEW method ($v_{max} = v_F$) for a fixed wave number $k = 0.1\sqrt{m\omega_p/\hbar}$. Comparison is made with the classical waterbag model and with the quantum-mechanical single-stream model ($v_{max} = \sqrt{\hbar\omega_p/m}$).

the Wigner distribution function for the zero-momentum CE wave function. The Wigner function, normalized to the particle number, is defined by

$$f(x,v) = \frac{n_0}{2\pi} \int_{-\infty}^{+\infty} \mathrm{d}r\ \psi\left(x+\frac{r}{2}\right)\psi^*\left(x-\frac{r}{2}\right)\ e^{-ivr}. \quad (10)$$

At wavebreaking the classical cold-plasma phase-space trajectory $v = v(x(a))$ develops a vertical slope, since

$$\frac{\partial v}{\partial x} = \frac{\partial v}{\partial a}\ \frac{1}{\partial x/\partial a} \quad (11)$$

approaches infinity when $\partial x/\partial a \to 0$. The broken wave develops a Z-shaped form as shown in fig. 3. Comparisons with classical PIC simulations, indicated by solid lines, show that the zero-momentum flow is most sensitive to breaking, while the streams with higher momenta only break later or at higher amplitudes. Wavebreaking amplitudes obtained in this manner are shown in fig. 4. The results are in excellent agreement with eq. (9), demonstrating that the classical waterbag model with the appropriate quantum-mechanical cut-off at $v_{max} = v_F$ accounts very well for the wavebreaking amplitudes in quantum plasmas. For more realistic 3d velocity distributions, v_{max} has to be replaced by the sound velocity c_0. This amounts to setting $\tilde{v} = c_0/v_{ph} = \sqrt{3/5}v_F/v_{ph}$ for a degenerate quantum plasma. Finally, it is noted that the wavebreaking limit defines the maximum fields for stationary waves but higher fields may be excited in nonstationary cases [7].

Although the quantum wavebreaking amplitudes closely follow the classical prediction with the appropriate sound velocity, specific nonclassical features can be observed in the broken-wave regime. These are most pronounced in the density distribution of the zero-momentum flow, shown in the inset of fig. 3. While the classical density peak is split into a double peak, the quantum-mechanical density distribution shows a single broad peak with side maxima. The different density profiles result from the cancellation of positive and negative parts in the Wigner distribution. To emphasize the differences between the classical and quantum-mechanical density distributions we have compared the densities for the single stream with initial momentum $\boldsymbol{p}_s = 0$, only. In the total density resulting from the multi-stream distribution these differences are much less pronounced.

To gain a more detailed understanding of the quantum interferences observed, we have studied wavebreaking by a single-stream model, consisting of a single CE wave with zero carrier momentum. It applies to a degenerate plasma at zero temperature with a Fermi energy of the order of the plasmon energy. The single-stream model yields the well-known dispersion relation [29]

$$\omega^2 = 1 + \frac{k^4}{4} \quad (12)$$

for small-amplitude oscillations. It shows that there exist two modes propagating at a given phase velocity $v_{ph} = \omega/k$ with the wave numbers

$$k^2 = 2v_{ph}^2(1 \pm \sqrt{1 - 1/v_{ph}^4}). \quad (13)$$

Stable propagation is limited to phase velocities $v_{ph} > 1$. In the waterbag model, the limit of small-amplitude propagation is given by $v_{ph} = v_{max}$. Since $v_{max} = 1$ corresponds to

$v_{max} = \sqrt{\hbar\omega_p/m}$, in usual units, the single-stream model can account for an effective Fermi energy of the order of the plasmon energy. At large phase velocities, the high-frequency mode (upper sign) corresponds to free-particle motion, the low-frequency mode (lower sign) to plasma oscillations at the plasma frequency. The nonlinear evolution of these modes can be described in the rest frame of the wave, moving with phase velocity $-v_{ph}$, by the set of stationary Madelung-Poisson equations,

$$\partial_z^2\phi = n - 1, \tag{14a}$$

$$\partial_z^2 A + (2\phi - v^2)A = 0, \tag{14b}$$

with $n = v_{ph}/v = A^2$ and $v = \partial_z S$, defined by the wave function $\psi = Ae^{iS}$. Note that eq. (14b) is the time-independent Schrödinger equation with the kinetic energy of the flow separated from the remaining kinetic energy. Neglecting $\partial_z^2 A$ corresponds to the quasiclassical approximation, leading to the cold-plasma wavebreaking amplitude E_{max}. In general, the quasiclassical approximation becomes violated at the wavebreaking point. We have numerically solved eqs. (14) by posing initial conditions in a minimum of the density ($\partial_z A = \partial_z \phi = 0$). The initial values for ϕ and A have been varied to obtain stationary solutions for at least 10 periods. If the initial minimum density gets lower than a critical value, the density develops interference fringes in the subsequent density maximum, similar to the ones seen in fig. 3. Taking this critical value as the criterion of wavebreaking, we find the maximum electric fields shown in fig. 4 by squared symbols. One can clearly see the qualitative agreement of the full quantum kinetic simulation with the single-stream model for stationary modes.

It is concluded that the CEW method allows one to study the quantum kinetic evolution of nonlinear plasma waves. Wavebreaking amplitudes can be predicted in accordance with a waterbag model with the appropriate quantum-mechanical cut-off. Moreover, it is found that wavebreaking amplitudes at negligible fluid pressure are limited quantum-mechanically by nonlinearly coupled plasmon and free-particle modes. The CEW method has been introduced here for a relatively simple 1d electrostatic model with periodic boundary conditions. However, due to its close conceptual relationship with the classical PIC method, it provides a perspective for a wider scope of beam plasma studies in the quantum kinetic regime. Two and three dimensions, electromagnetic interactions, inhomogeneous and bounded systems as well as correlated systems based on the quantum Boltzmann equation [11] are well conceiveable as promising fields for the extension of the computational method in forthcoming work.

REFERENCES

[1] Ichimaru S., *Rev. Mod. Phys.*, **54** (1982) 1017.
[2] Glenzer S. H. and Redmer R., *Rev. Mod. Phys.*, **81** (2009) 1625.
[3] Thiele R., Sperling P., Chen M., Bornath T., Fäustlin R. R., Fortmann C., Glenzer S. H., Kraeft W.-D., Pukhov A., Toleikis S., Tschentscher T. and Redmer R., *Phys. Rev. E*, **82** (2010) 056404.
[4] Dawson J. M., *Phys. Rev.*, **113** (1959) 383.
[5] Coffey T. P., *Phys. Fluids*, **14** (1971) 1402.
[6] Kruer W. L., *Phys. Fluids*, **22** (1979) 1111.
[7] Bergmann A. and Mulser P., *Phys. Rev. E*, **47** (1993) 3585.
[8] Katsouleas T. and Mori W. B., *Phys. Rev. Lett.*, **61** (1988) 90.
[9] Schroeder C. B., Esarey E. and Shadwick B. A., *Phys. Rev. E*, **72** (2005) 055401.
[10] Dawson J. M., *Rev. Mod. Phys.*, **55** (1983) 403.
[11] Uehling E. A. and Uhlenbeck G. E., *Phys. Rev.*, **43** (1933) 552.
[12] Kremp D., Bornath T., Bonitz M. and Schlanges M., *Phys. Rev. E*, **60** (1999) 4725.
[13] Klimontovich Y. and Silin V., *Sov. Phys. Dokl.*, **82** (1952) 361.
[14] Klimontovich Y. and Silin V., *Sov. Phys. JETP*, **23** (1952) 151.
[15] Lindhard J., *K. Dan. Vidensk. Selsk. Mat.-Fys. Medd.*, **28**, No. 8 (1954).
[16] Wigner E., *Phys. Rev.*, **40** (1932) 749.
[17] Fennel T., Meiwes-Broer K.-H., Tiggesbäumker J., Reinhard P.-G., Dinh P. M. and Suraud E., *Rev. Mod. Phys.*, **82** (2010) 1793.
[18] Kelbg G., *Ann. Phys.* (*Lepzig*), **467** (1963) 219.
[19] Deutsch C., *Phys. Lett. A*, **60** (1977) 317.
[20] Filinov A. V., Bonitz M. and Ebeling W., *J. Phys. A: Math. Gen.*, **36** (2003) 5957.
[21] Jakob B., Reinhard P.-G., Toepffer C. and Zwicknagel G., *Phys. Rev. E*, **76** (2007) 036406.
[22] Suh N.-D., Feix M. R. and Bertrand P., *J. Comput. Phys.*, **94** (1991) 403.
[23] Bonitz M., Scott D. C., Binder R. and Koch S. W., *Phys. Rev. B*, **50** (1994) 15095.
[24] Shukla P. K. and Eliasson B., *Plasma Phys. Control. Fusion*, **52** (2010) 124040.
[25] Bloch F., *Z. Phys.*, **81** (1933) 363.
[26] Tokatly I. and Pankratov O., *Phys. Rev. B*, **60** (1999) 15550.
[27] Haas F., Manfredi G. and Feix M., *Phys. Rev. E*, **62** (2000) 2763.
[28] Manfredi G. and Haas F., *Phys. Rev. B*, **64** (2001) 075316.
[29] Drummond J. E., *Plasma Physics* (McGraw-Hill Book Company Inc., New York) 1961.
[30] Crank J. and Nicolson P., *Proc. Camb. Phil. Soc.*, **43** (1947) 50.